Hindawi Publishing Corporation
International Journal of Photoenergy
Volume 2012, Article ID 492746, 8 pages
doi:10.1155/2012/492746

Research Article

Effects of Composition and Calcination Temperature on Photocatalytic H_2 Evolution over $Cd_{1-x}Zn_xS/SiO_2$ from Glycerol and Water Mixture

Cancan Fan, Xitao Wang, Huanxin Sang, and Fen Wang

Tianjin Key Laboratory of Applied Catalysis Science and Technology, College of Chemical Engineering and Technology, Tianjin University, Tianjin 300072, China

Correspondence should be addressed to Xitao Wang, wangxt@tju.edu.cn

Received 12 October 2011; Accepted 3 February 2012

Academic Editor: Leonardo Palmisano

A series of sulfide coupled semiconductors supported on SiO_2, $Cd_{1-x}Zn_xS/SiO_2$ ($x = 0 \sim 1$), was prepared by incipient wet impregnation method. The photocatalysts were characterized by XRD, XPS, TPR, and UV/Vis DRS. Characterization results show that the chemical actions between ZnS and CdS resulted in the formation of $Cd_{1-x}Zn_xS$ solid solutions on the surface of the support and the formation of them is affected by the molar ratio of ZnS/CdS and calcination temperature. Performance of photocatalysts was tested in the home made reactor under both UV light and solar-simulated light irradiation by detecting the rate of the photocatalytic H_2 evolution from glycerol solution. The hydrogen production rates are related to the catalyst composition, surface structure, photoabsorption property, as well as the amount of solid solution. The maximum rate of hydrogen production, 550 μmol·h^{-1} under UV light irradiation and 210 μmol·h^{-1} under solar-simulated light irradiation, was obtained over $Cd_{0.8}Zn_{0.2}S/SiO_2$ solid solution calcined at 723 K.

1. Introduction

The production of hydrogen has received a lot of attention because of its potential application as a clean energy vector. However, the industrial hydrogen production consumes a large amount of fossil fuels and also results in huge emissions of CO_2 [1]. Scientists and engineers have devoted numerous efforts [2–4] to the eco-friendly hydrogen production methods. Among those methods that are outside of C-cycle, photocatalytic hydrogen production by water splitting using solar energy which is famous for abundant resource, low cost, and zero pollution has been intensively investigated. For the sake of photocatalytic hydrogen production enhancement, a lot of techniques have been studied [5–9], such as modifying photocatalyst and adding chemical additives to water. When it comes to chemical additives, sulfide/sulfite is the most common and effective sacrificial agent and has been well studied [4, 10, 11]. Recently, the sacrificial agents have been extended to organics [12, 13], and now using glycerol as sacrificial agent is gaining significance for its overproduction as the by-product of the chemical reaction transforming vegetable oil to biodiesel [14], and adding glycerol to help enhance hydrogen production efficiency is an economic way to convert waste product to useful material.

The design of the catalyst plays a crucial role in the process of water splitting. Since photoinduced decomposition of water on TiO_2 electrodes has been discovered [15], the semiconductor-based photocatalysts including metal sulfides, especially chalcogenides of IIB, such as CdS and ZnS have attracted extensive interest. CdS, whose band gap is 2.42 ev and flat potential is −0.87 V (vsNHE) [16], is a promising visible light responsive photocatalyst for hydrogen production [17]. Nevertheless, the recombination of the photogenerated electrons and holes is still a considerable drawback. In order to improve the photoactivity of CdS, vast efforts have been devoted to the study of CdS preparation or modification, and fruitful achievements have been got, such as the formation of the size-quantized CdS nanocrystals

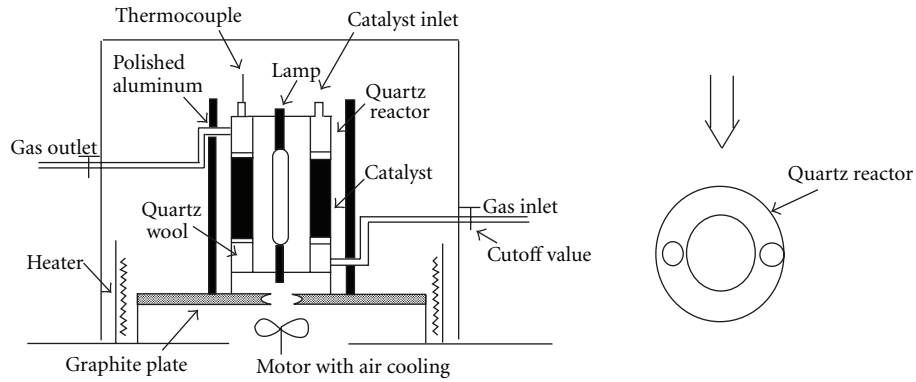

Figure 1: Reactor for photocatalytic H_2 evolution from glycerol solution.

[6, 18], loading noble metals [7, 19], and coupling CdS with other semiconductors [12, 20]. Even some of the composite semiconductors form solid solutions instead of being simply coupled [20]. These solid solutions exhibit superior advantages to single ones. Xu et al. has reported the fabrication of $Zn_xCd_{1-x}S$ solid solutions by sulfuring the precursors [21]. Villoria et al. has reported the influence of thermal treatment to the photoactivity of $Cd_{1-x}Zn_xS$ solid solutions in hydrogen production from aqueous solutions containing $S^{2-}/SO_3{}^{2-}$ as sacrificial agents [22]. However, the effects of the composition and thermal treatment on the $Cd_{1-x}Zn_xS$ solid solutions that are finely dispersed on SiO_2 and their ability of hydrogen production from water-glycerol solution have not been studied.

In this work, we aim to study the effect of the composition and thermal treatment on the formation of $Cd_{1-x}Zn_xS$ solid solutions and the photocatalytic activity of the designed catalysts.

2. Experiment

2.1. Preparation of the $Cd_{1-x}Zn_xS/SiO_2$ *Catalysts.* Spherical SiO_2 (d = 1.0 mm, S_{BET} = 350 m^2/g), bought from Qingdao Haiyang Chemical Co., was used as the supporter after being washed in dilute HNO_3 solution, then washed in deionized water for three times, and dried at 473 K under vacuum.

The precursors of coupled-semiconductor CdS-ZnS/SiO_2 with total loading of CdS and ZnS 20 wt.% were prepared by isometric impregnating spherical SiO_2 with the mixture solution of $Cd(NO_3)_2$ and $Zn(NO_3)_2$ at room temperature. After the impregnation, the sample was kept inside the seal flask for 4 h at 323 K, and then the sample was dried at 393 K for 12 h. The as-prepared sample was impregnated by a slight access of Na_2S solution to form sulfide semiconductors. The sample was washed by a large amount of deionized water to remove excessive S^{2-}, then dried at 393 K for 12 h, and calcined at 723 K for 4 h. The CdS-ZnS/SiO_2-coupled semiconductors with different Cd/Zn molar ratio were prepared, marked as $Cd_{1-x}Zn_xS/SiO_2$ (x = 0, 0.2, 0.4, 0.6, 0.8, and 1), respectively.

In order to investigate the effect of calcination temperature on the performance of CdS-ZnS/SiO_2 coupledsemiconductors, the $Cd_{0.8}Zn_{0.2}S/SiO_2$ samples calcined at 623 K, 673 K, 723 K, and 773 K were prepared.

2.2. Characterization. X-ray diffractometer (XRD) of the samples was recorded on a D/MAX-2500 automatic powder diffractometer equipped with the graphite monochromatized Cu Kα radiation flux at a scanning rate of 0.02°/s and in the 2θ range of 10–60°. X-ray photoelectron spectroscopy (XPS) measurements were recorded with an SSX-100/206 probe, using non-monochromatized Al-Mg Kα X-ray as the excitation source. UV-Vis spectra were recorded on a PerkinElmer Lamdba35 spectrophotometer at room temperature. H_2-temperature programmed reduction (TPR) experiments were carried out in a flow reactor system, in which 50 mg of catalyst was charged each run into a U-shaped quartz microreactor (6 mm i.d.). The sample was reduced in a 5% H_2/He stream (30 mL/min). The reduction temperature was raised uniformly from 373 K to 1223 K at a ramp of 10°C/min. H_2 consumption was measured by a thermal conductivity detector (TCD).

2.3. Photocatalytic Activity Evaluation. The photocatalytic reaction was carried out in a fixed bed flow type annular quartz reactor with inner diameter 34 mm and outer diameter 38 mm as shown in Figure 1. In a typical reaction, 3 g catalyst was loaded in the reactor and then 5 mL 5% glycerol-water mixture was added dropwise. The temperature of the irradiated surface of the catalyst was monitored by a thermocouple directly inserted into the catalyst bed. UV irradiation was performed by the use of a high-pressure Hg lamp (Power: 125 W, Intensity: 40 m W/m^2), which was located in the center of the reactor. Simulated solar irradiation was performed by the Xe-arc lamp (Power: 500 W, Intensity: 750 m W/m^2), also located in the center of a reactor (inner diameter 65 mm and outer diameter 69 mm) with an external cooling jacket. Ar flow of 20 mL/min passed through the reactor to collect and transfer gaseous products to the analysis system. The irradiated catalyst surface temperature, under both the UV light and simulated solar irradiation, was

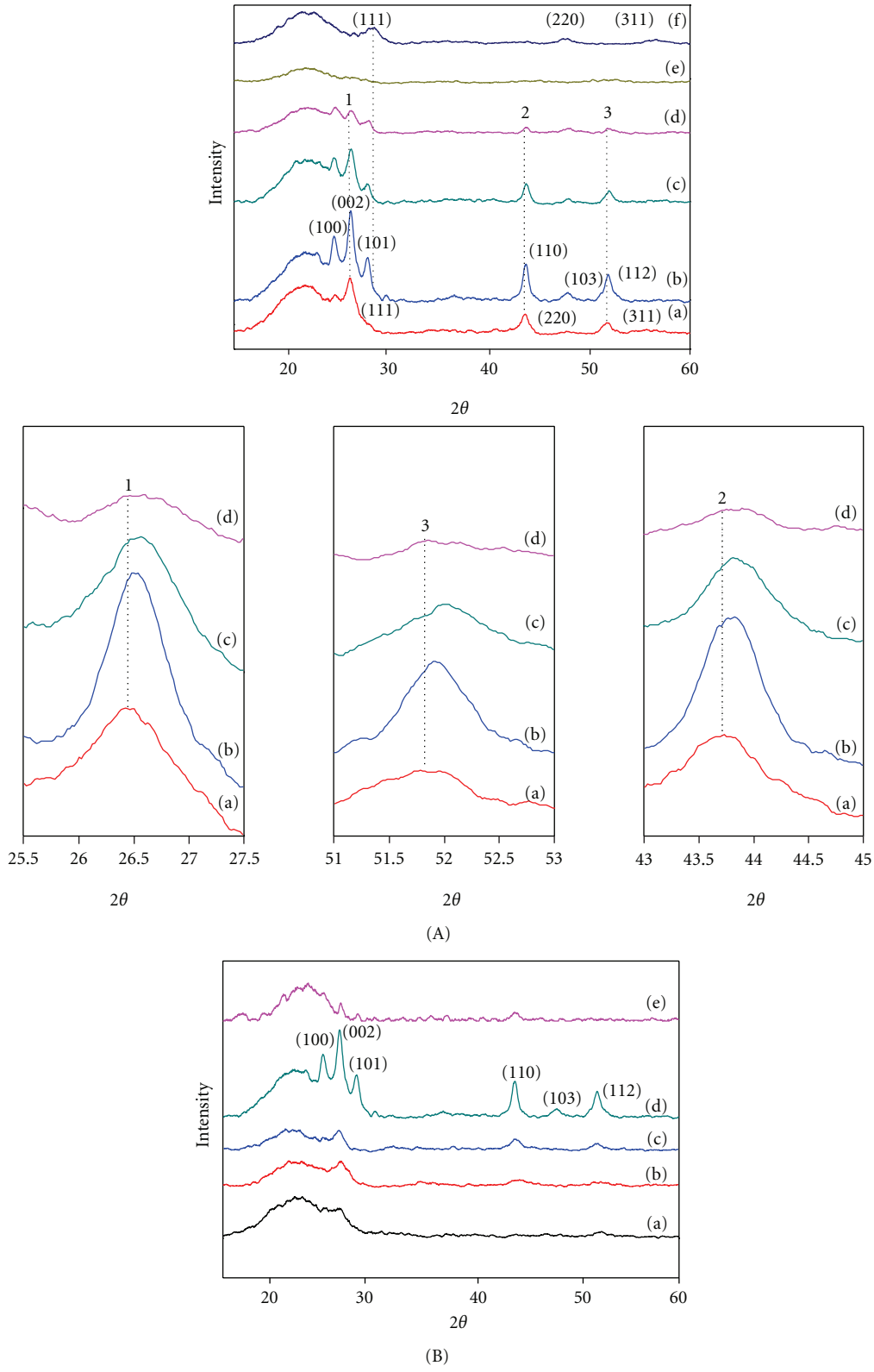

FIGURE 2: XRD patterns of $Cd_{1-x}Zn_xS/SiO_2$ samples with different composition (A): (a) $x = 0$, (b) $x = 0.2$, (c) $x = 0.4$, (d) $x = 0.6$, (e) $x = 0.8$, and (f) $x = 1$ and of $Cd_{0.8}Zn_{0.2}S/SiO_2$ sample calcined at different temperature (B): (a) 393 K, (b)623 K, (c)673 K, (d)723 K, and (e)773 K.

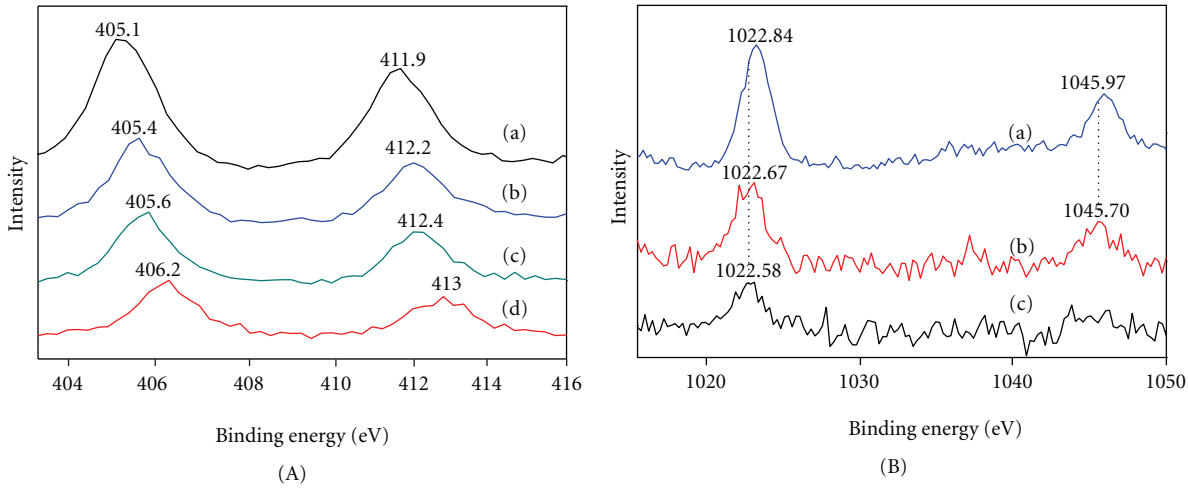

FIGURE 3: XPS spectra of Cd $3d_{5/2}$ and $3d_{3/2}$ of $Cd_{1-x}Zn_xS/SiO_2$ with different composition (A): (a) $x = 0$, (b) $x = 0.2$, (c) $x = 0.4$, and (d) $x = 0.6$ and XPS spectra of Zn $2p_{3/2}$ and $2p_{1/2}$ of $Cd_{1-x}Zn_xS/SiO_2$ series (B): (a) $x = 1$, (b) $x = 0.8$, and (c) $x = 0.6$.

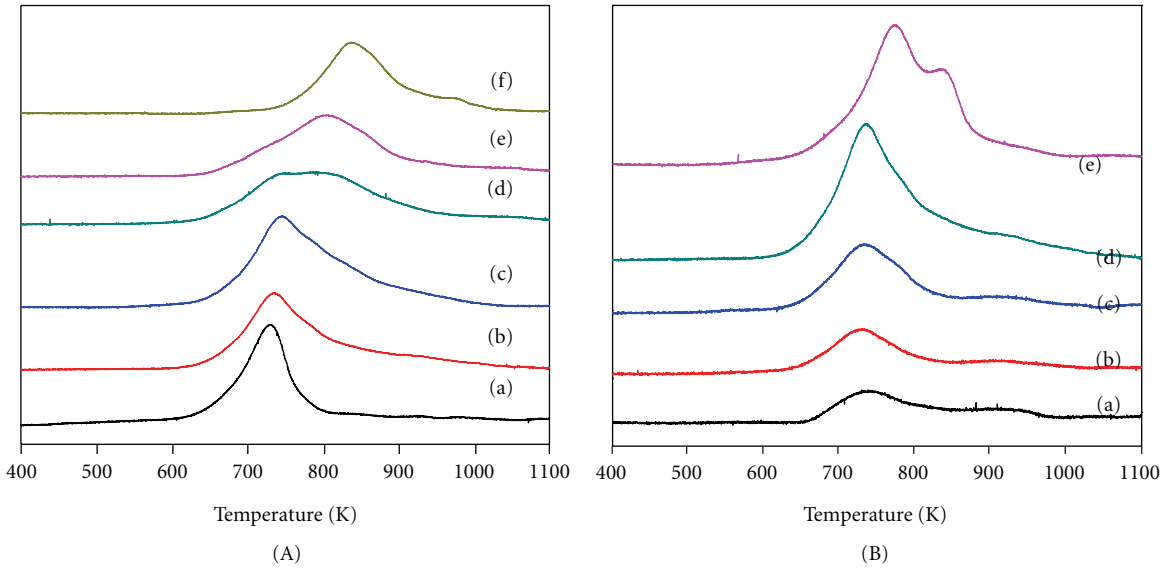

FIGURE 4: TPR profiles of $Cd_{1-x}Zn_xS/SiO_2$ with different composition (A): (a) $x = 0$, (b) $x = 0.2$, (c) $x = 0.4$, (d) $x = 0.6$, (e) $x = 0.8$, and (f) $x = 1$ and of $Cd_{0.8}Zn_{0.2}S/SiO_2$ sample calcined at different temperature (B): (a) 393 K, (b)623 K, (c)673 K, (d)723 K, and (e)773 K.

313 K. The products of reaction were analyzed in situ by gas chromatography (GC) using thermal conductivity cell.

The hydrogen production rate is calculated according to following formula:

$$\text{Hydrogen production rate } \left(\frac{\mu\text{mol}}{h}\right) = \frac{\text{H}_2\%(\text{v/v}) \times \text{flow rate}(20\,\text{mL/min}) \times 60 \times 1000}{22.41(\text{L/mol})}. \quad (1)$$

3. Results and Discussion

3.1. Structure and Composition of $Cd_{1-x}Zn_xS/SiO_2$*-Coupled Semiconductors.* The XRD patterns of the as-prepared $Cd_{1-x}Zn_xS/SiO_2$-coupled semiconductors with different composition were shown in Figure 2(A). All of the XRD patterns show size-broadening effects, indicating the finite size of these nanocrystals. For CdS/SiO_2, the peaks at d values of 1.7, 2.0, and 3.3 corresponding to the (311), (220), and (111) planes with the lattice constant $a = 5.82$, show the presence of cubic crystalline phase CdS (JCPDS no. 10-0454). The ZnS/SiO_2 is characterized by the sphalerite structure (JCPDS 5-566) with the reflections of (111), (220), and (311). As for $Cd_{1-x}Zn_xS/SiO_2$, six prominent peaks, which can be indexed to the diffraction from (100), (002), (101), (110), (103), and (112) lattice planes of hexagonal wurtzite structure crystal $Cd_{1-x}Zn_xS$ solid solution, were observed. The XRD peaks shift to larger angles gradually as the Zn content increases, which also indicates that the $Cd_{1-x}Zn_xS/SiO_2$ has formed

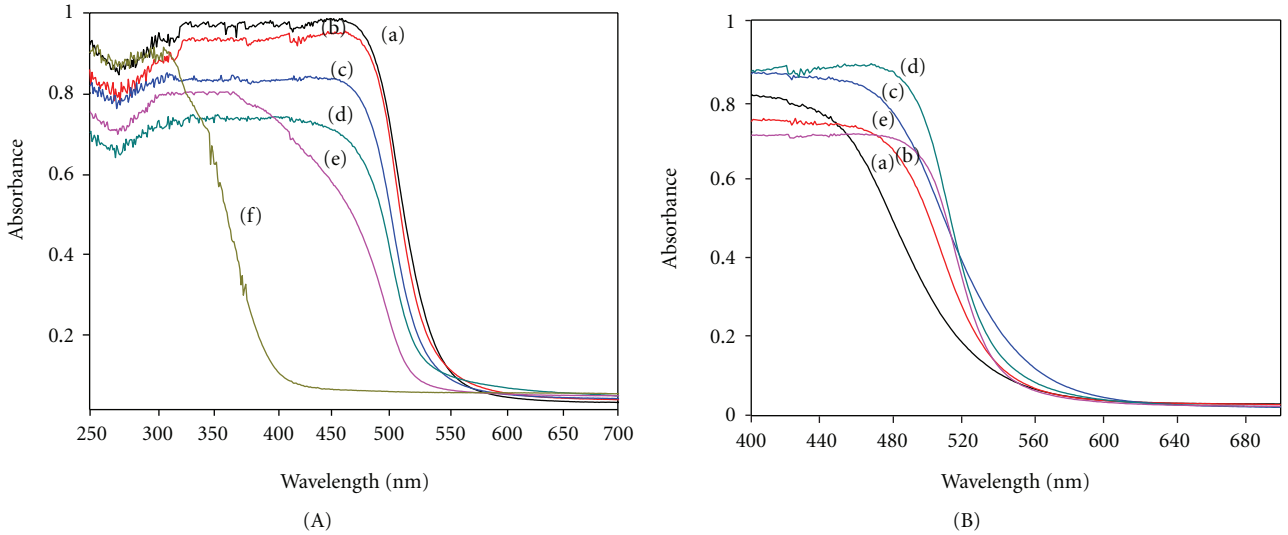

FIGURE 5: UV-Vis DRS spectra of $Cd_{1-x}Zn_xS/SiO_2$ with different composition (A): (a) $x = 0$, (b) $x = 0.2$, (c) $x = 0.4$, (d) $x = 0.6$, (e) $x = 0.8$, and (f) $x = 1$ and of $Cd_{0.8}Zn_{0.2}S/SiO_2$ sample calcined at different temperature (B): (a) 393 K, (b) 623 K, (c) 673 K, (d) 723 K, and (e) 773 K.

solid solutions instead of being simply mixed. It is also obvious that the intensity of the diffraction peaks varies with the change of the composition of solid solutions.

Figure 2(B) shows the XRD patterns of $Cd_{0.8}Zn_{0.2}S/SiO_2$ catalysts calcined at 393 K, 573 K, 623 K, 723 K, and 773 K, respectively. When the temperature is lower than 723 K, the XRD patterns of $Cd_{0.8}Zn_{0.2}S/SiO_2$ exhibit only weak characterization peaks of cubic crystalline phase CdS, no signals of $Cd_{0.8}Zn_{0.2}S$ solid solution with wurtzite structure are detected. The CdS diffraction peaks become more and more distinct with the increase of the calcination temperature, which means that the increase in calcinations temperature helps the formation of sulfide and solid solution. When the temperature reached to 773 K, the diffraction peaks corresponding to the $Cd_{0.8}Zn_{0.2}S$ solid solution disappeared, and only CdS can be observed, which demonstrate that the $Cd_{0.8}Zn_{0.2}S$ solid solution undergoes decomposition at higher calcination temperature.

To gain deeper insight into the surface constitution and properties of these samples, their Zn2p, Cd3d, and S2p binding energies were investigated. The corresponding spectra of Zn2p and Cd3d are plotted in Figure 3. The position of the S2p signal for $Cd_{1-x}Zn_xS/SiO_2$ samples is at around 161.5 eV (not shown), which is similar to the value of Zn–S and Cd–S bonds in the literature [23]. For CdS/SiO_2 sample, the observed binding energy of Cd ($3d_{5/2}$) is 405.1 eV and that of Cd ($3d_{3/2}$) is 411.9 eV, which agrees with values reported for divalent cadmium in sulphides [21, 23, 24]. The peak positions, corresponding to binding energies, of Cd (3d) are progressively shifted to lower values with the increase of Zn : Cd ratio. A similar situation can also be observed in the case of Zn (2p) peaks whose binding energy 1022.8 eV corresponds to the value reported mainly for divalent zinc in sulphides [23, 24] that are shifted to higher values of binding energies with the increase of Zn : Cd ratio. From these results, we can conclude that some of the cadmium atoms are replaced by zinc atoms. In other words, the solid solutions of CdS and ZnS are formed.

The TPR profiles of $Cd_{1-x}Zn_xS/SiO_2$ catalysts were shown in Figure 4. It can be seen from Figure 4(A) that the TPR profiles of 20% CdS/SiO_2 and ZnS/SiO_2 display two peaks at 730 K and 840 K, respectively, which is due to the reduction of Cd^{2+} and Zn^{2+}. For the $Cd_{1-x}Zn_xS/SiO_2$ sample ($x = 0.2$, 0.4, 0.6, 0.8), only one reduction peak can be detected, and the peaks are shifted gradually to higher reduction temperature. These results confirm that the solid solutions of CdS and ZnS were formed.

Figure 4(B) shows the effects of calcination temperature on the composition and structure of $Cd_{0.8}Zn_{0.2}S/SiO_2$ samples. $Cd_{0.8}Zn_{0.2}S/SiO_2$ sample calcined below 773 K shows one peak, which corresponds to the reduction of the solid solution. The peak area augments with the increase of the calcination temperature, indicating the increase of the amount of sulfide and solid solution on the surface of the sample. When the calcination temperature is up to 773 K, the sample shows two reduction peaks. According to the results of XRD and TPR of CdS/SiO_2 and ZnS/SiO_2 samples, the peak at lower temperature can be due to the reduction of CdS, while the other one can be indexed to the reduction of ZnS. These results indicate that the solid solution has begun to decompose at higher temperature.

3.2. Optical Properties of $Cd_{1-x}Zn_xS/SiO_2$*-Coupled Semiconductors.* Figure 5(A) presents the UV-Vis DRS spectra of $Cd_{1-x}Zn_xS/SiO_2$-coupled semiconductors, which reveals the significant effects of the sample composition on the optical absorption behaviors. The band edge of the ZnS/SiO_2 sample locates around 400 nm, which hardly belongs to visible light

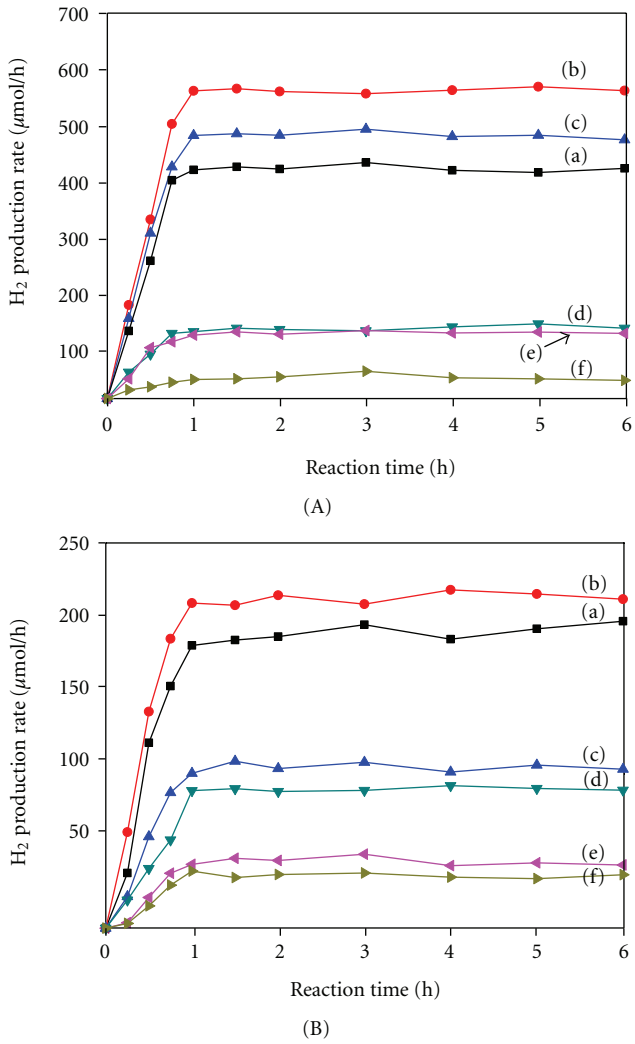

Figure 6: Rates of the photocatalytic H_2 evolution from glycerol solution (5%) over $Cd_{1-x}Zn_xS/SiO_2$ samples under UV light (A) and visible light (B): (a) $x = 0$, (b) $x = 0.2$, (c) $x = 0.4$, (d) $x = 0.6$, (e) $x = 0.8$, (f) $x = 1$.

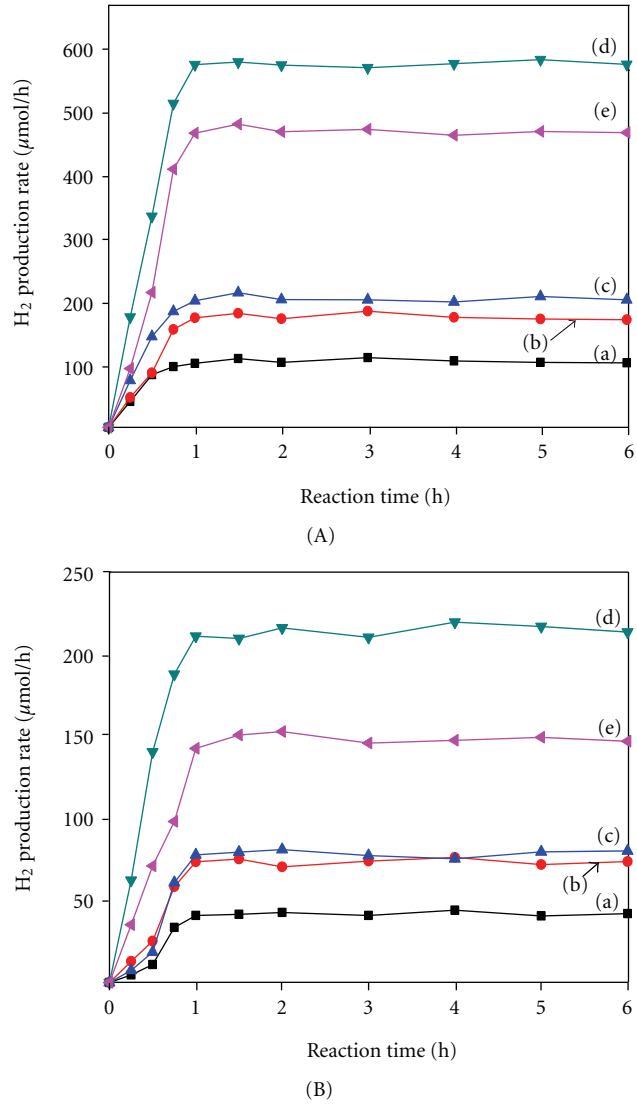

Figure 7: Rates of the photocatalytic H_2 evolution from glycerol solution (5%) over $Cd_{0.8}Zn_{0.2}S/SiO_2$ calcined at different temperatures under UV light (A) and visible light (B): (a) 393 K, (b) 623 K, (c) 673 K, (d) 723 K, (e) 773 K.

absorption. In the UV-vis DRS spectra of $Cd_{1-x}Zn_xS/SiO_2$, the absorption edge of each solid solution was gradually red shifted to visible light district with the increasing amount of Cd and distributed between that of CdS and ZnS. The photoabsorption for visible light at the range of 400–550 nm was enhanced with the increase of Cd : Zn ratio.

Figure 5(B) also shows that the photoabsorption of $Cd_{0.8}Zn_{0.2}S/SiO_2$ first increases and then decreases with the increase of calcination temperature. The sample calcined at 723 K exhibits a maximum photoabsorption at the range of visible light area (around 400–500 nm), which is due to the higher content of $Cd_{0.8}Zn_{0.2}S$ solid solution on the surface of the sample.

According to the characterization results mentioned previously, it can be seen that the composition and the amount of solid solution play an important role in optical absorption behaviors of $Cd_{1-x}Zn_xS/SiO_2$ catalysts.

3.3. Photocatalytic Activity

3.3.1. Effects of the Composition on Photocatalytic Performance. Photocatalytic hydrogen evolution studies are conducted on the $Cd_{1-x}Zn_xS/SiO_2$ series catalysts from 5%(V/V) glycerol-water mixtures under UV and solar simulated light irradiation. The results obtained are shown in Figure 6. It is observed that the rates of hydrogen production on all the catalysts reach a maximum at 60 min and then show a steady state even after 6-hour prolonged irradiation. The activity of the ZnS/SiO_2 under UV and visible irradiation was quite low. However, after the addition of the CdS, the hydrogen yields are enhanced under both UV and solar-simulated light irradiation. The photocatalytic activity of the $Cd_{1-x}Zn_xS/SiO_2$ first increases and then decreases with the increase of CdS. The $Cd_{0.8}Zn_{0.2}S/SiO_2$ sample exhibits a

maximum H_2 production of 550 μmol·h^{-1}under UV light irradiation and 210 μmol·h^{-1} under solar-simulated light irradiation. This can be attributed to the effects of surface phase composition of the formed solid solutions on (a) the charging behavior of the semiconductor surface, (b) the photoabsorption behaviors, and (c) the positions of the valence- and conduction-band levels of the semiconductor, which highly affect the redox ability. The coupled semiconductors promote the separation of the photoinduced electrons and holes, which results in a better photocatalytic performance than that of individual components. Although the addition of the higher band gap semiconductor ZnS is disadvantageous to light absorption, it elevates the conduction band position of the catalyst, which is very important to the enhancement of the hydrogen production.

3.3.2. Effects of the Calcination Temperature on Photocatalytic Performance. The effect of calcination temperature on the reaction rate has been investigated over a set of five $Cd_{0.8}Zn_{0.2}S/SiO_2$ photocatalysts under UV light irradiation and solar-simulated light irradiation. Typical results obtained are shown in Figure 7, where the rates of hydrogen production are plotted against irradiation time. Comparison of results presented in Figure 7 shows that calcination temperature affects substantially the rate of H_2 evolution. The hydrogen production rate increases with the increase of calcination temperature and reaches a maximum at 723 K and then decreases with the further temperature increase. It is known that the changes of the rates of the photocatalytic H_2 evolution with calcination temperature are related with the surface composition and the amount of $Cd_{0.8}Zn_{0.2}S$ solid solution, while, according to the characterization results of TPR, XRD, and UV/Vis DRS, the amount of $Cd_{0.8}Zn_{0.2}S$ solid solution increases with the increase of the calcination temperature from 393 k to 723 K and then decreases obviously at 773 K due to the decomposition of solid solution.

4. Conclusions

We have demonstrated that the supported $Cd_{1-x}Zn_xS/SiO_2$ (x = 0.2∼0.8) solid solutions can be prepared by incipient wet impregnation and found that the surface structure and photoabsorption of the solid solutions vary with the change of the composition. With the adding of ZnS, the solid solutions have worse photoabsorption but better redox ability. As a balance of the two main effects, the $Cd_{0.8}Zn_{0.2}S/SiO_2$ catalyst has the best photoactivity, 550 μmol·h^{-1}under UV light irradiation and 210 μmol·h^{-1} under solar-simulated light irradiation. Moreover, the thermal treatment has an important influence on the formation of the solid solution. Before 723 K, increasing calcination temperature helps to form $Cd_{0.8}Zn_{0.2}S$ solid solution. However, when the temperature is up to 773 K, the solid solution begins to decompose. The hydrogen production rates of the $Cd_{0.8}Zn_{0.2}S/SiO_2$ series calcinated under different temperature are consistent with the amount of the solid solution.

Acknowledgment

The authors acknowledge the financial supports from the National Natural Science Foundation of China (20806059).

References

[1] R. Abe, "Recent progress on photocatalytic and photoelectrochemical water splitting under visible light irradiation," *Journal of Photochemistry and Photobiology C*, vol. 11, no. 4, pp. 179–209, 2010.

[2] W. Grochala and P. P. Edwards, "Thermal decomposition of the non-interstitial hydrides for the storage and production of hydrogen," *Chemical Reviews*, vol. 104, no. 3, pp. 1283–1315, 2004.

[3] P. V. Kamat, "Meeting the clean energy demand: nanostructure architectures for solar energy conversion," *Journal of Physical Chemistry C*, vol. 111, no. 7, pp. 2834–2860, 2007.

[4] C. Xing, Y. Zhang, W. Yan, and L. Guo, "Band structure-controlled solid solution of $Cd_{1-x}Zn_xS$ photocatalyst for hydrogen production by water splitting," *International Journal of Hydrogen Energy*, vol. 31, no. 14, pp. 2018–2024, 2006.

[5] N. Meng, M. K. H. Leung, D. Y. C. Leung, and K. Sumathy, "A review and recent developments in photocatalytic water-splitting using TiO_2 for hydrogen production," *Renewable and Sustainable Energy Reviews*, vol. 11, no. 3, pp. 401–425, 2007.

[6] B. A. Korgel and H. G. Monbouquette, "Quantum confinement effects enable photocatalyzed nitrate reduction at neutral pH using CdS nanocrystals," *Journal of Physical Chemistry B*, vol. 101, no. 25, pp. 5010–5017, 1997.

[7] S. H. Shen, L. Guo, X. Chen, F. Ren, and S. S. Mao, "Effect of Ag_2S on solar-driven photocatalytic hydrogen evolution of nanostructured CdS," *International Journal of Hydrogen Energy*, vol. 35, no. 13, pp. 7110–7115, 2010.

[8] H. I. Kim, J. Kim, W. Kim, and W. Choi, "Enhanced photocatalytic and photoelectrochemical activity in the ternary hybrid of $CdS/TiO_2/WO_3$ through the cascadal electron transfer," *Journal of Physical Chemistry C*, vol. 115, no. 19, pp. 9797–9805, 2011.

[9] V. M. Daskalaki and D. I. Kondarides, "Efficient production of hydrogen by photo-induced reforming of glycerol at ambient conditions," *Catalysis Today*, vol. 144, no. 1-2, pp. 75–80, 2009.

[10] A. Koca and M. Sahin, "Photocatalytic hydrogen production by direct sun light from sulfide/sulfite solution," *International Journal of Hydrogen Energy*, vol. 27, no. 4, pp. 363–367, 2002.

[11] R. Priya and S. Kanmani, "Solar photocatalytic generation of hydrogen under ultraviolet-visible light irradiation on $(CdS/ZnS)/Ag_2S$ + (RuO_2/TiO_2) photocatalysts," *Bulletin of Materials Science*, vol. 33, no. 1, pp. 85–88, 2010.

[12] M. Vasileia, M. Antoniadou, G. Li Puma, D. I. Kondarides, and P. Lianos, "Solar light-responsive $Pt/CdS/TiO_2$ photocatalysts for hydrogen production and simultaneous degradation of inorganic or organic sacrificial agents in wastewater," *Environmental Science and Technology*, vol. 44, no. 19, pp. 7200–7205, 2010.

[13] Y. Chen, H. Yang, X. Liu, and L. Guo, "Effects of cocatalysts on photocatalytic properties of la doped Cd_2TaGaO_6 photocatalysts for hydrogen evolution from ethanol aqueous solution," *International Journal of Hydrogen Energy*, vol. 35, no. 13, pp. 7029–7035, 2010.

[14] F. Ma and M. A. Hanna, "Biodiesel production: a review," *Bioresource Technology*, vol. 70, no. 1, pp. 1–15, 1999.

[15] A. Fujishima and K. Honda, "Electrochemical photolysis of water at a semiconductor electrode," *Nature*, vol. 238, no. 5358, pp. 37–38, 1972.

[16] D. Meissner, R. Memming, and B. Kastening, "Photoelectrochemistry of cadmium sulfide reanalysis of photocorrosion and flat-band potential," *Journal of physical chemistry*, vol. 92, no. 12, pp. 3476–3483, 1988.

[17] N. Z. Bao, L. M. Shen, T. Takata, and K. Domen, "Self-templated synthesis of nanoporous CdS nanostructures for highly efficient photocatalytic hydrogen production under visible light," *Chemistry of Materials*, vol. 20, no. 1, pp. 110–117, 2008.

[18] A. Kumar and S. Mital, "Synthesis and photophysics of 6-dimethylaminopurine-capped Q-CdS nanoparticles - A study of its photocatalytic behavior," *International Journal of Photoenergy*, vol. 6, no. 2, pp. 61–68, 2004.

[19] M. Berr, A. Vaneski, A. S. Susha et al., "Colloidal CdS nanorods decorated with subnanometer sized Pt clusters for photocatalytic hydrogen generation," *Applied Physics Letters*, vol. 97, no. 9, Article ID 093108, 2010.

[20] I. Tsuji, H. Kato, and A. Kudo, "Visible-light-induced H2 evolution from an aqueous solution containing sulfide and sulfite over a ZnS-$CuInS_2$-$AgInS_2$ solid-solution photocatalyst," *Angewandte Chemie*, vol. 44, no. 23, pp. 3565–3568, 2005.

[21] X. Xu, R. Lu, X. Zhao et al., "Fabrication and photocatalytic performance of a $Zn_xCd_{1-x}S$ solid solution prepared by sulfuration of a single layered double hydroxide precursor," *Applied Catalysis B*, vol. 102, no. 1-2, pp. 147–156, 2010.

[22] J. A. Villoria, R. M. Navarro Yerga, S. M. Al-Zahrani, and J. L. G. Fierro, "Photocatalytic hydrogen production on $Cd_{1-x}Zn_xS$ solid solutions under visible light: influence of thermal treatment," *Industrial and Engineering Chemistry Research*, vol. 49, no. 15, pp. 6854–6861, 2010.

[23] S. Celebi, A. K. Erdamar, A. Sennaroglu, A. Kurt, and H. Y. Acar, "Synthesis and characterization of poly(acrylic acid) stabilized cadmium sulfide quantum dots," *Journal of Physical Chemistry B*, vol. 111, no. 44, pp. 12668–12675, 2007.

[24] A. Deshpande, P. Shah, R. S. Gholap, and N. M. Gupta, "Interfacial and physico-chemical properties of polymer-supported CdS/ZnS nanocomposites and their role in the visible-light mediated photocatalytic splitting of water," *Journal of Colloid and Interface Science*, vol. 333, no. 1, pp. 263–268, 2009.